Quantitative Analysis of Extracardiac Versus Intraatrial Fontan Anatomic Geometries

Resmi KrishnankuttyRema, MS, Lakshmi P. Dasi, PhD, Kerem Pekkan, PhD,* Kartik Sundareswaran, MS, Mark Fogel, MD, Shiva Sharma, MD, Kirk Kanter, MD, Thomas Spray, MD, and Ajit P. Yoganathan, PhD

Wallace H. Coulter School of Biomedical Engineering, Georgia Institute of Technology, Atlanta, Georgia; Children's Hospital of Philadelphia, Philadelphia, Pennsylvania; Pediatric Cardiology Services, Lawrenceville, and Emory University, Atlanta, Georgia

Background. **There exists large geometric variability among total cavopulmonary connections (TCPC) because of the patient-specific anatomies and the chosen surgical procedure. In this study we present quantitative comparison of the geometric characteristics of the extracardiac and intraatrial Fontan anatomies, the two commonly used TCPC procedures.**

Methods. **A method of centerline approximation of the three-dimensional geometries (skeletonization) was used to quantify the TCPC geometric parameters such as vessel areas, curvature, and collinearity. The TCPC anatomies of 26 patients, 13 extracardiac and 13 intraatrial, were analyzed in this study.**

Results. **There was no significant difference in the vessel dimensions between extracardiac and intraatrial TCPCs, with the overall magnitudes agreeing well with that seen in normal children except for the inferior vena cava. Intraatrial baffles had significant fluctuations in cross-sectional area along the length of the baffle as opposed to extracardiacs ($p < 0.05$). Patients with hypoplastic left heart syndrome had significant narrowing of the left pulmonary artery ($p < 0.05$), suggesting a possible physical constriction from the reconstructed aorta.**

Conclusions. **This study benchmarks the anatomic variability of patient-specific TCPCs. Intraatrial Fontan geometries have significant difference in the area variations across the vessel length compared with the extracardiac geometry. Also, patients with hypoplastic left heart are at a higher risk of left pulmonary artery narrowing.**

(Ann Thorac Surg 2008;85:810–7)

The Fontan procedure is a palliative cure for children born with a single functional ventricle [1]. In this procedure the surgeon creates a complex two-inlet, two-outlet vessel junction (total cavopulmonary connection, TCPC) to reroute venous return from the superior and inferior venae cavae (SVC, IVC) to the left and right pulmonary arteries (LPA, RPA) [2]. The right side of the heart is thus bypassed, with the single functioning ventricle pumping blood through the systemic and pulmonary circuits in series. Although this procedure reduces mortality rate, its long-term outcome is considered far from optimal owing to the inherent nonoptimal nature of a two-inlet, two-outlet junction from an energy loss standpoint. Consequently, several studies addressed the hemodynamics of the TCPC connection [3–7], with the overarching objective of designing an energy-efficient connection. Nevertheless, the anatomy of TCPC connections in vivo is yet to be quantified and analyzed, a step necessary for fundamental insight into the observed complex hemodynamics, which will not only help surgeons to differentiate among the several variants (templates) of the TCPC but also guide engineers to design superior energy-efficient connections.

The two commonly used surgical options for the TCPC procedure are the lateral intraatrial (IA) tunnel and the extracardiac (EC) conduit connection. In IA, the IVC is routed through the right atrium, whereas in EC an external conduit is routed around the right atrium to make the connection [2]. Although procedurally well differentiated, their geometries have never been compared quantitatively. As mentioned above, the lack of quantitative geometric characterization of these complex vascular anatomies hinders analysis necessary to correlate these surgical techniques to the overall hemodynamic performance of these TCPC templates.

In this study, geometric characteristics of patient-specific TCPC anatomies are studied retrospectively in 26 patients (13 ECs and 13 IAs each). Characteristics such as vessel area, curvature, and offset are quantified and compared to benchmark the anatomic differences between EC and IA types of connections with important clinical implications.

Patients and Methods

Patient Selection

Twenty-six patients, 13 each of EC and IA, were selected from a magnetic resonance imaging database of Fontan

Accepted for publication Nov 28, 2007.

*Currently at the Department of Biomedical Engineering, Carnegie Mellon University, Pittsburgh, PA.

Address correspondence to Dr Yoganathan, Wallace H. Coulter School of Biomedical Engineering, Georgia Institute of Technology, Room 2119 U.A. Whitaker Building, 313 Ferst Drive, Atlanta, GA 30332–0535; e-mail: ajit.yoganathan@bme.gatech.edu.

Published by Elsevier Inc

0003-4975/08/$34.00
doi:10.1016/j.athoracsur.2007.11.082

Abbreviations and Acronyms

EC = extracardiac
HLHS = hypoplastic left heart syndrome
IA = intraatrial
IVC = inferior vena cava
LPA = left pulmonary artery
PA = pulmonary artery
RPA = right pulmonary artery
SVC = superior vena cava
TCPC = total cavopulmonary connection
3D = three-dimensional

patients (http://fontan.bme.gatech.edu). The database is part of a National Institutes of Health–funded ongoing study for understanding Fontan hemodynamics. All patients were imaged either at Children's Hospital of Philadelphia or at Emory University/Children's Healthcare of Atlanta. Informed consent was obtained from all patients, and all study protocols complied with the institutional review boards of participating hospitals and the Georgia Institute of Technology. The inclusion criteria for this study were (1) availability of experimental and computational fluid dynamics power loss data to enable future correlations between geometry and hemodynamics (not studied in this paper); and (2) availability of clinical information necessary to categorize each study group. Anatomic reconstructions with visible artifacts (some geometries had loss of magnetic resonance imaging signal owing to the presence of clips in the vessels from surgery) were excluded from the study group.

Among the 13 EC patients, 2 were from Emory University/Children's Healthcare of Atlanta and 11 were from Children's Hospital of Philadelphia, whereas among the IA patients, 4 were from Emory University/Children's Healthcare of Atlanta and 9 were from Children's Hospital of Philadelphia. Clinical details of the studied EC and IA patient populations are provided in Table 1. All 26 patients are doing well clinically. For all 26 patients,

Table 1. Clinical Diagnosis of Patients With Extracardiac and Intraatrial Fontan Repair

Patient	Diagnosis	Second Stage	BSA (m^2)	Age (y)	Interval Between Fontan and MRI Scan (y)
Extracardiac TCPC					
CHOA007	HLHS	BDG	0.79	6	3
CHOA008	HRV, TA	BDG	0.69	5	2
CHOP006	HLHS	Hemi	1.05	10	8
CHOP007	HRV, Ebstein's anomaly	BDG	1.02	8	2
CHOP013	HLHS	Hemi	0.83	6	4.5
CHOP067	DI-LV, PS, TGA	BDG	1.064	9	7
CHOP085	HLHS	BDG	0.589	3	0.5
CHOP088	DX, TA, TGA, AA hypoplasia	BDG	0.544	3	0.5
CHOP089	TA, VSD	BDG	0.872	7	5.5
CHOP090	PA, IVS, RV hypertrophy	BDG	1.152	8	6.5
CHOP091	DO-RV, IVS, MA, PA	BDG	0.994	8	7
CHOP095	DI-LV, PA	BDG	1.253	8	6
CHOP116	Ebstein's anomaly	BDG	0.793	8	2
Intraatrial TCPC					
CHOA004	HRV, TA, VSD, PS	BDG	0.56	3	0.5
CHOA009	SV-DI AV connection	BDG	0.58	2	0.25
CHOA011	HLHS	BDG	1.21	11	8
CHOA027	HRV, TGA, TA, VSD, LPA hypoplasia	BDG	0.58	2	0.25
CHOP008	HLHS	Hemi	1.94	16	15.5
CHOP018	HLHS	Hemi	1.23	12	9.5
CHOP030	TA, VSD	Hemi	1.32	10	9
CHOP034	HRV, DX, TA, VSD, PS	Hemi	1.19	11	7
CHOP037	PA, HRV	Hemi	1.49	15	16
CHOP068	HLHS	Hemi	0.94	6	4.5
CHOP073	HLHS	Hemi	0.963	9	7
CHOP092	HLHS, TGA, hypoplastic AA, VSD	Hemi	0.495	1	0.25
CHOP096	PA	BDG	1.063	10	8

AA = aortic arch; ASD = atrial septal defect; AV = atrioventricular; BDG = bidirectional Glenn; BSA = body surface area; DI = double inlet; DO = double outlet; DX = dextrocardia; Hemi = hemi-Fontan; HLHS = hypoplastic left heart syndrome; HRV = hypoplastic right ventricle; IVS = intact ventricular septum; LV = left ventricle; MA = mitral atresia; MRI = magnetic resonance imaging; PA = pulmonary atresia; PS = pulmonary stenosis; RV = right ventricle; SV = single ventricle; TA = tricuspid atresia; TCPC = total cavopulmonary connection; TGA = transposition of great arteries; VSD = ventricular septal defect.

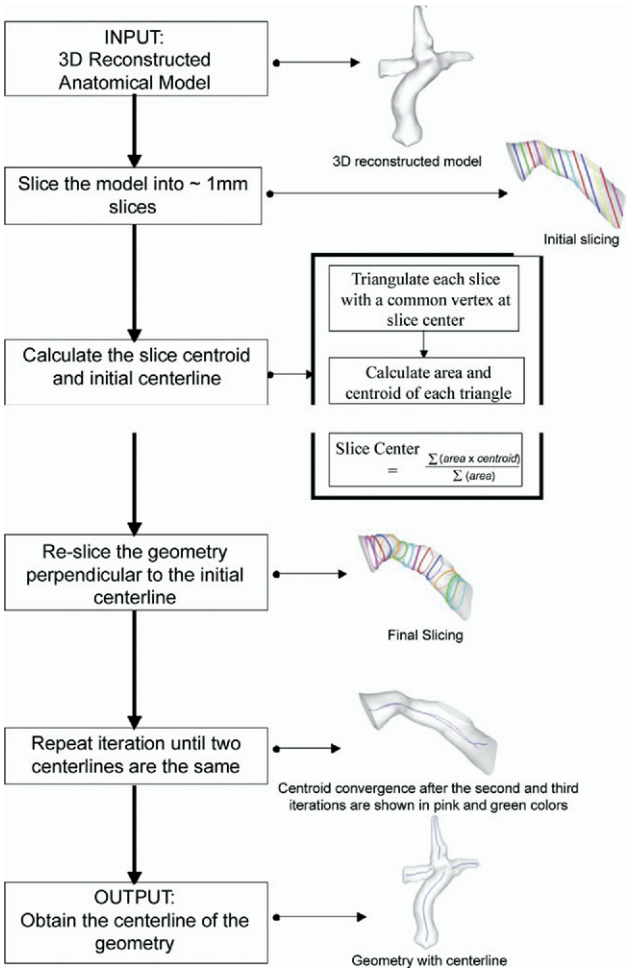

Fig 1. Flow chart representation of the skeletonization procedure. Starting with the three-dimensional (3D) reconstructed anatomic model, the flow chart shows pictures of initial and final slicing directions, converged centerlines, and the final skeleton of the geometry.

geometric characterization of the TCPC was performed to quantitatively differentiate EC and IA patients. Because the patient population may be partitioned with respect to lesion type, a detailed analysis between two categories, hypoplastic left heart syndrome (HLHS) and non-HLHS, was also performed.

Geometric Analysis

To characterize the complex three-dimensional (3D) geometries of the TCPCs, a skeletonization approach was used. Skeletonization is a widely used technique to analyze geometries of tubular body organs (eg, [8–15]). First, the full 3D TCPC anatomy was reconstructed from the raw stack of magnetic resonance imaging data and represented as a 3D surface geometry [16, 17] for each patient. These patient-specific surface representations were then reduced to their respective skeletal representation using the skeletonization approach (procedure outlined in Fig 1).

The 3D surface representation of the TCPC was sliced at approximately 1-mm spacing in the magnetic resonance imaging left-right and superior-inferior coordinate directions, thus generating sections that were roughly perpendicular to the LPA and RPA and IVC and superior vena cava (SVC). The centroids of these cross sections were computed and connected to generate an initial estimate of the vessel centerline (each vessel segment was treated separately to simplify the computational scheme). Because this approximation was poor in regions where the sectioning significantly departs from the true cross section of the vessel, the centerline was iteratively refined as follows: for each subsequent iteration, the 3D vessel geometry was resliced in direction perpendicular to the tangent of the centerline curve. The centroids were recomputed for the new slices, and the curve through the newly computed centroids provided a better estimate of the true centerline. The centroid curve was found to converge within four iterations to the true vessel centerline. A flowchart representation of the skeletonization is shown in Figure 1.

Computation of Geometric Characteristics

Several geometric characteristics of TCPCs were computed from the skeletonized representation. These include vessel area characteristics, vessel curvature at the TCPC junction, and vessel offset.

VESSEL AREA CHARACTERISTICS. The cross-sectional area of each vessel section from the final iteration provides the variation of the vessel area along the centerline. Vessel area characteristics for each patient were computed, namely mean, standard deviation, and minimum and maximum vessel area along the vessel segment. The vessel segment corresponds the vessel between the points where the vessel meets the junction to an anatomic landmark. The landmark for the pulmonary arteries (PAs) was the point of bifurcation, whereas the landmark for the SVC and IVC were the locations of the innominate and hepatic veins, respectively (Fig 2).

The area standard deviation is a measure of the geometric inhomogeneities along the vessel length. The minimum vessel area can be used to quantify vessel narrowing (such as a stenosis), especially in PAs.

VESSEL ORIENTATION AND CURVATURE. The tangent vector, T, and its derivative, $\dot{T}$, were numerically calculated with second-order accuracy at the point where the vessel intersects with the junction. The curvature of the vessel centerlines at the TCPC junction was then calculated as follows:

$$\kappa = \left|T \times \dot{T}\right| / \left|T\right|^3 \quad (1)$$

To quantify the extent to which the IVC and SVC are oriented in a head-on collinear manner, we defined a collinearity measure, ϕ, of the TCPC as follows:

$$\phi = \frac{1}{2}\left(\left|\hat{T}_{ivc} \times \hat{r}\right| + \left|\hat{T}_{svc} \times \hat{r}\right|\right) \quad (2)$$

where $\hat{T}$ is the unit tangent vector of the corresponding vessel and $\hat{r}$ is the unit displacement vector between the points where the IVC and SVC meet the junction. By

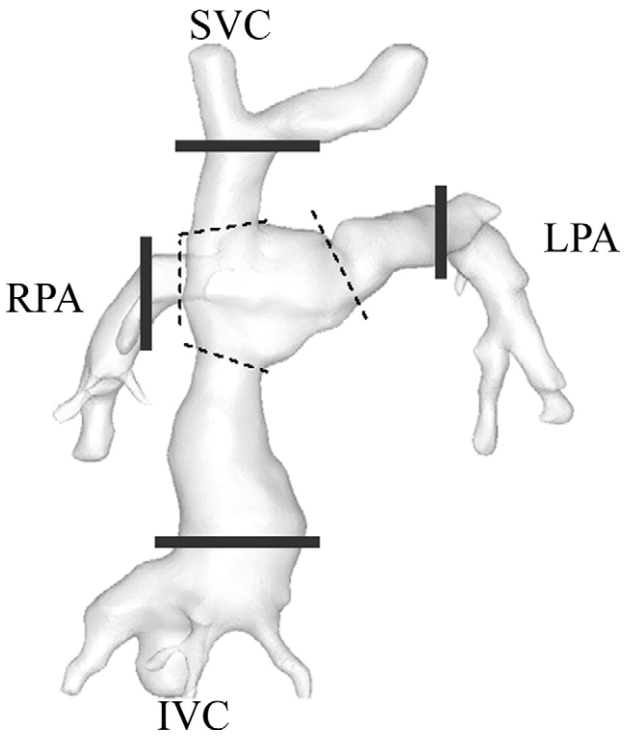

Fig 2. Three-dimensional reconstructed total cavopulmonary connection anatomy with an illustration of the various vessel segments defined between the points where the vessels meet the junction (dotted lines) and the anatomic landmarks (solid lines). (IVC = inferior vena cava; LPA = left pulmonary artery; RPA = right pulmonary artery; SVC = superior vena cava.)

definition, $0 \leq \phi \leq 1$, where $\phi = 0$ corresponds to a head-on colliding orientation between the great veins, and $\phi = 1$ corresponds to a configuration where the SVC and IVC are both anastomosed parallel to the PAs. Figure 3 shows the schematic of curvature and collinearity computation.

VESSEL OFFSET CHARACTERISTICS. Two vessel offsets were defined for each of the 3D reconstructed anatomies: (1) anteroposterior offset between IVC and SVC, and (2) right-left offset between IVC and SVC. These were computed by projecting the displacement vector r along the anteroposterior and right-left directions.

Statistical Analysis

Because the data were not normally distributed and corresponded to a two-sample population (EC versus IA), the nonparametric Mann-Whitney U test was used to examine statistical significance among the various geometric variables evaluated. Differentiating factors are considered statistically significant for probability values less than 0.05.

Results

Figure 4 shows the 3D surface geometries and skeletonizations of the 13 EC and 13 IA patient groups, detailing their large geometric variability and complexity. Table 2 provides the geometric variables calculated from the data reduction process described above. All the geometric variables have been normalized by patient body surface area.

Vessel Area Characteristics

The mean and standard deviation of vessel areas computed for the EC and IA patient groups are shown in Figure 5, along with published nomograms for healthy children [18–21] (Fig 5A). As seen in Figure 5A, there was no statistical significance in the vessel dimensions between ECs and IAs, with the overall magnitudes agreeing well with that expected in normal children except for IVC. The IVC baffle size was almost double that of the normal dimensions. Standard deviations of the cross-sectional area computed along the vessel length, on the other hand, revealed statistically significant differences between the two groups with regard to the IVC area variation ($p = 0.0006$; Fig 5B). Another statistically significant difference ($p = 0.04$) was observed in the ratios of mean cross-sectional areas of RPA to SVC between the EC and IA (Fig 5C).

Figure 6 shows the comparison of minimum PA sizes (ie, smallest cross section along the length of the skeletonized PA) between EC and IA as well as HLHS and non-HLHS patient groupings. As seen in Figure 6A, there

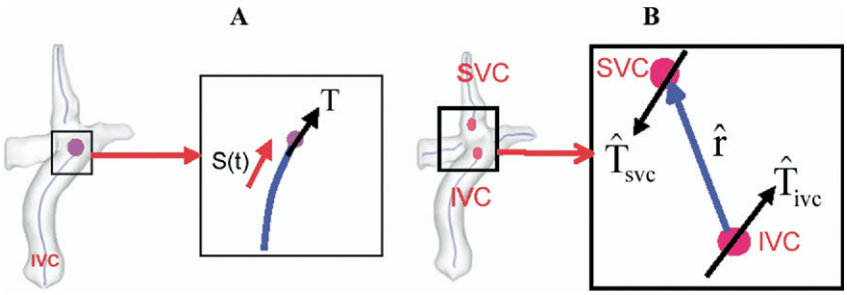

Fig 3. Schematic explaining the terms used for (A) curvature and (B) collinearity calculation is shown. Sample total cavopulmonary connection geometry with the skeleton of the venae cavae is shown on the left and total cavopulmonary connection junction is enlarged on the right (black box). (A) T is the tangent vector (black arrow) at the total cavopulmonary connection junction, and the red arrow indicates the direction of the space curve S(t), which is the inferior vena cava (IVC) centerline in this scenario. (B) Unit tangent vectors $\hat{T}_{svc}$ and $\hat{T}_{ivc}$ are shown in black arrows, and the unit displacement vector $\hat{r}$ is shown in blue arrow. (SVC = superior vena cava.)

Table 2. Summary of the Computed Values of Geometric Characteristics for 13 Extracardiac and 13 Intraatrial Geometries

Computed Variables	Extracardiac	Intraatrial	*p* Value
Mean vessel cross-sectional area/BSA			
IVC ($\times 10^{-4}$)	3.67 ± 1.83	4.03 ± 1.71	0.29
SVC ($\times 10^{-4}$)	1.65 ± 0.67	1.34 ± 0.63	0.08
RPA ($\times 10^{-4}$)	1.18 ± 0.70	1.19 ± 0.62	0.29
LPA ($\times 10^{-4}$)	1.12 ± 0.59	0.95 ± 0.41	0.17
Vessel cross-sectional area ratio			
LPA/IVC	0.32 ± 0.19	0.27 ± 0.15	0.25
LPA/SVC	0.69 ± 0.34	0.79 ± 0.42	0.14
RPA/IVC	0.34 ± 0.15	0.31 ± 0.12	0.15
RPA/SVC	0.72 ± 0.28	0.89 ± 0.26	0.04
Vessel area standard deviation/BSA			
IVC ($\times 10^{-5}$)	3.42 ± 1.96	9.17 ± 4.55	0.0006
SVC ($\times 10^{-5}$)	4.17 ± 1.29	3.23 ± 1.7	0.09
RPA ($\times 10^{-5}$)	2.38 ± 1.39	2.95 ± 2.13	0.44
LPA ($\times 10^{-5}$)	3.51 ± 2.22	3.89 ± 1.80	0.27
Minimum vessel cross-sectional area/BSA			
RPA ($\times 10^{-5}$)	7.99 ± 5.97	7.71 ± 4.64	0.35
LPA ($\times 10^{-5}$)	6.57 ± 4.64	4.71 ± 2.92	0.11
Vessel curvature at the TCPC junction			
IVC	0.19 ± 0.11	0.26 ± 0.19	0.21
SVC	0.22 ± 0.19	0.18 ± 0.16	0.41
RPA	0.34 ± 0.43	0.22 ± 0.26	0.07
LPA	0.21 ± 0.17	0.16 ± 0.11	0.35
IVC-SVC collinearity	0.54 ± 0.11	0.48 ± 0.28	0.05
IVC-SVC AP offset/$BSA^{1/2}$ ($\times 10^{-3}$)	3.44 ± 3.4	2.36 ± 1.81	0.17
IVC-SVC RL offset/$BSA^{1/2}$ ($\times 10^{-3}$)	4.6 ± 3.01	4.47 ± 4.33	0.29
PA-VC offset/$BSA^{1/2}$ ($\times 10^{-3}$)	7.01 ± 2.01	7.51 ± 2.64	0.46

AP = anteroposterior; BSA = body surface area; IVC = inferior vena cava; LPA = left pulmonary artery; PA = pulmonary artery; RL = right-left; RPA = right pulmonary artery; SVC = superior vena cava; TCPC = total cavopulmonary connection; VC = venae cavae.

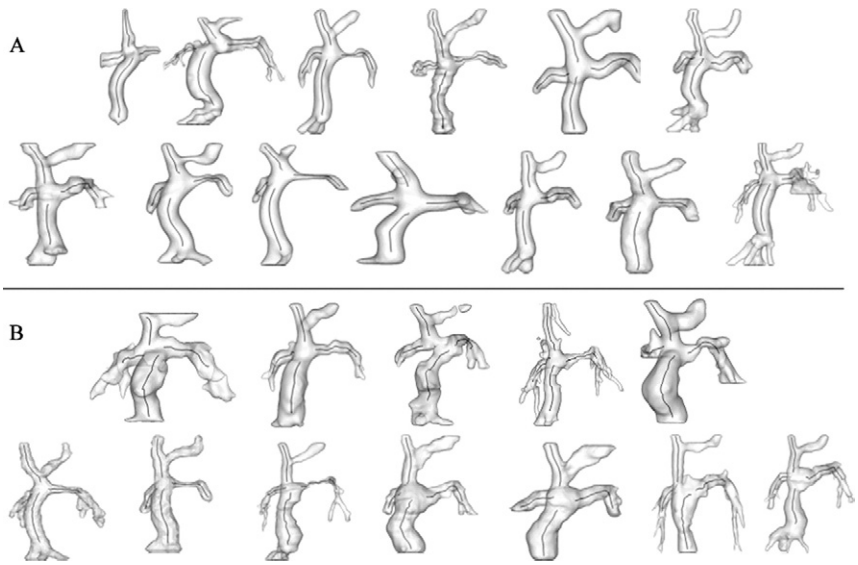

Fig 4. Three-dimensional reconstructed total cavopulmonary connection anatomies with centerline curves for extracardiac (A) and intraatrial (B) geometries.

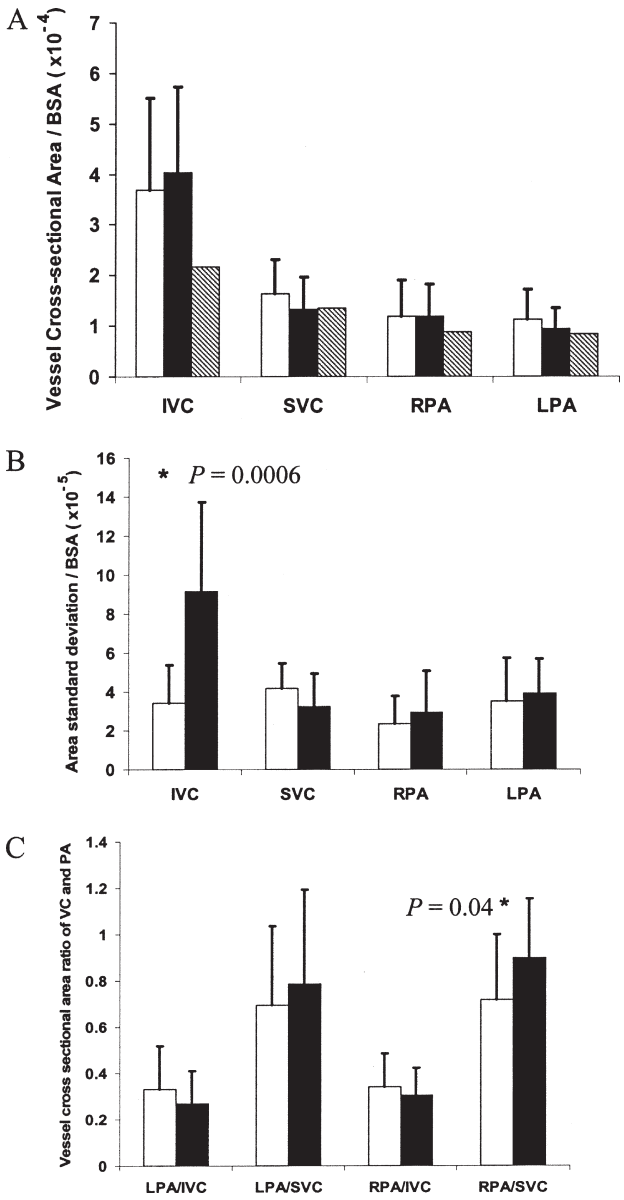

Fig 5. Vessel area characteristics with mean (A) and standard deviation (B) of each vessel in the vicinity of the total cavopulmonary connection and (C) vessel area ratios between the superior and inferior venae cavae (SVC, IVC) and left and right pulmonary arteries (LPA, RPA) compared between extracardiac (white bars) and intraatrial (black bars) patient groups (n = 13 each). Gray bars represent values for normal children. (BSA = body surface area; PA = pulmonary artery; VC = venae cavae.)

exists no significant difference between EC and IA with respect to minimum PA sizes. However, within the IA population, the minimum LPA size was significantly lower (p = 0.01) than the minimum RPA size. Figure 6B shows that the minimum LPA size for HLHS patients was significantly lower than that of non-HLHS patients (p = 0.01). Furthermore, the minimum LPA size was also observed to be significantly smaller than the minimum RPA size within the HLHS patient group (p = 0.01).

Comparison between the minimum PA sizes for the four possible independent subsets within the patient population, ie, IA-HLHS, IA-non-HLHS, EC-HLHS, and EC-non HLHS, is shown in Figure 6C.

Vessel Orientation, Curvature, and Offset

Figure 7 shows the mean vessel collinearity and curvature plotted between the EC and IA patient groups.

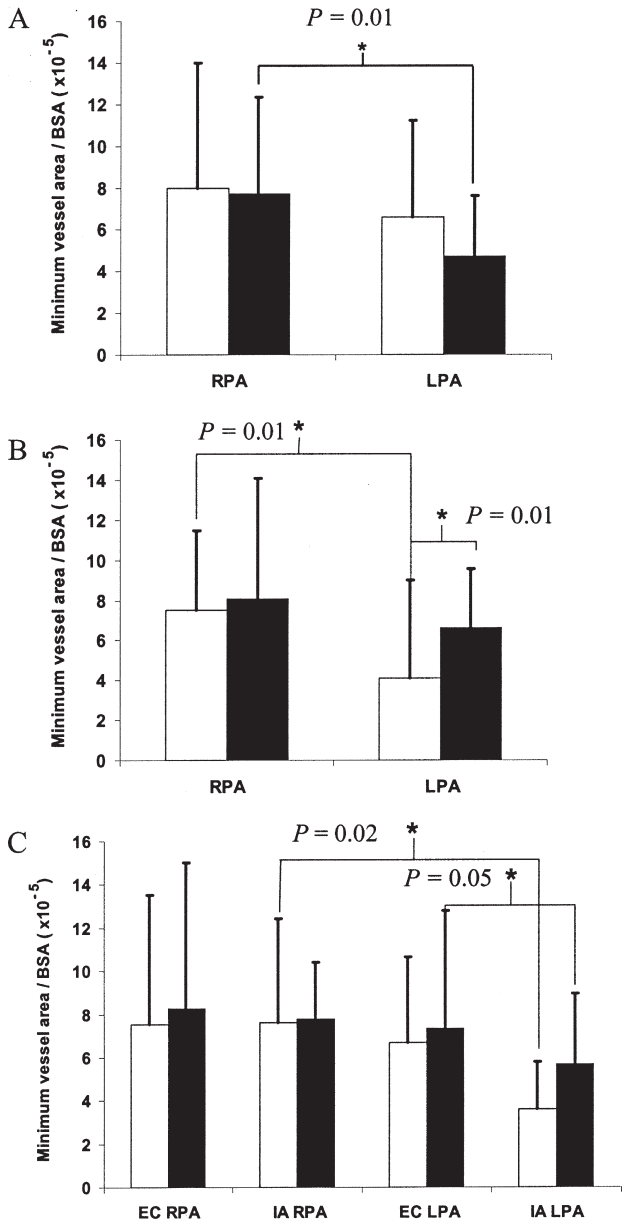

Fig 6. Minimum vessel area for left and right pulmonary arteries (LPA and RPA) for population groups: (A) extracardiac (white bars) and intraatrial (black bars; n = 13 each); (B) hypoplastic left heart syndrome (HLHS; white bars; n = 10) and non-HLHS (black bars; n = 16); and (C) extracardiac (EC) HLHS (white bars; n = 4), intraatrial (IA) HLHS (white bars; n = 6), extracardiac non-HLHS (black bars; n = 9), and intraatrial non-HLHS (black bars; n = 7). (BSA = body surface area.)

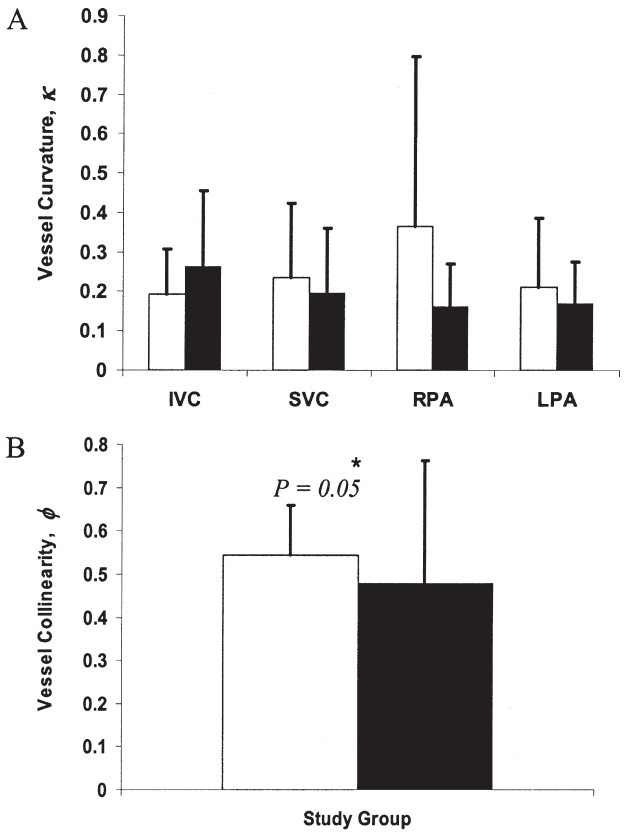

Fig 7. Total cavopulmonary connection orientation depicted by mean collinearity (A) and mean vessel curvature (B) between the extracardiac (white bars) and intraatrial (black bars) patient groups. (IVC = inferior vena cava; LPA = left pulmonary artery; RPA = right pulmonary artery; SVC = superior vena cava.)

All the vessel curvatures were roughly between 0.2 and 0.4 in magnitude, with fluctuations as large as 0.4. As seen in Figure 7A, the RPA curvature for the EC group was found to have larger patient-to-patient variation. Figure 7B shows significantly smaller collinearity measure for IAs than ECs ($p = 0.05$). Comparison between the vessel offsets showed no statistical significance (Table 2).

Comment

We quantified and compared the geometric characteristics of different types of Fontan anatomies between the EC and IA templates. Extracardiac and IA anatomies result from the two different approaches of constructing the Fontan baffle [2, 4]. However, our results show that there is no significant difference in the cross-sectional areas of IVC baffle for both patient groups. Instead, the difference appears to be a higher standard deviation of the baffle cross-sectional area along the vessel length in IA TCPCs compared with EC TCPCs (Fig 5A). Thus, it may be concluded that the IA baffle always has larger cross-sectional fluctuations than the EC conduit, which is expected as the former is constructed using part of the right atrium whereas a smooth and uniform graft conduit is used for the latter. The large standard deviation of the IVC cross-sectional areas observed in the IA TCPCs could also be the reason why there was no statistical significance between the IVC dimensions in IAs and ECs. No trends in the standard deviations of LPA and RPA could be detected. Also the vessel dimensions of SVC, LPA, and RPA were comparable with that of the normal children [18–20]. However, the IVC baffle size was almost double the size when compared with normal children. The large size of the IVC baffles was in fact intentionally chosen to incorporate the growth potential of the IVC. To see how the baffle size varies with time in both cases, we have plotted IVC cross-sectional area as a function of the interval between Fontan surgery and the magnetic resonance imaging scan date. This is shown in Figure 8. These data show that IA baffles grow as the patients grow older whereas the baffle growth is less for EC patients.

Intraatrial patients showed significantly higher values in the ratio of mean cross-sectional areas of RPA to SVC, which is possibly because the TCPC junction for the IA and EC is not located at the same point on the native PA. The location on the PA where the TCPC is constructed for the IA is possibly more toward the main PA.

Results in Figure 6 show that the minimum LPA size (region of smallest cross-sectional area) depends on both the patient's single-ventricle disease (HLHS or non-HLHS) and also the surgical protocol (EC or IA). From Figure 6C it is clear that among HLHS patients, the LPA had a significantly smaller ($p = 0.02$) minimum cross-sectional area than the RPA for the patients with IA connection. The trend is the same for HLHS patients who underwent EC surgery, too, but there is no statistical significance ($p = 0.15$). For non-HLHS patients, the minimum LPA cross-sectional area was smaller for patients with an IA TCPC than for those with an EC TCPC ($p = 0.05$). Precise reasons for this observation cannot be discerned from these data; additional clinical information of each operation is therefore needed. Nevertheless, HLHS patients appear to be at an increased risk of exhibiting LPA stenosis.

The high occurrence of LPA stenosis in the HLHS group could be attributed to the aortic reconstruction

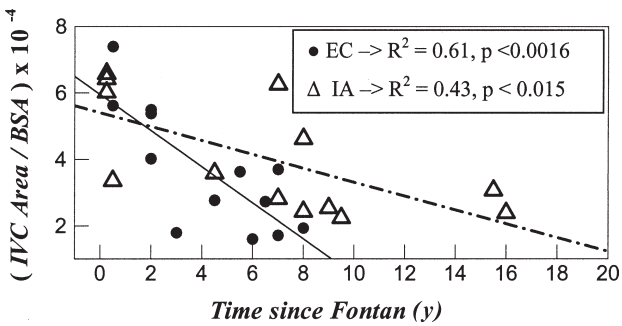

Fig 8. Inferior vena cava (IVC) baffle area normalized with body surface area (BSA) plotted as a function of time since Fontan. The solid line is the linear fit for extracardiac (EC), and the dashed line is for the intraatrial (IA) geometry.

procedure, because in almost all cases stenosis in the LPA occurred right underneath the location of the reconstructed aorta. Thus, one explanation could be that the reconstructed aorta possibly introduces nonphysiologic contact stresses on the LPA. Therefore, as the patient grows, the LPA is constricted, giving rise to a stenosis.

There was no statistical significance in the curvature of the vessels at the meeting point of the TCPC junction. The reason for the large standard deviation in the curvature of the RPA may be attributed to a particular geometry, as shown in Figure 4, in which the RPA was more curved than the other anatomies.

As depicted in Figure 7A, the IA Fontan procedures have lower collinearity (nearly significant) value than their EC counterparts. Collinearity values approaching 0 can be interpreted as having their IVC and SVC oriented in a head-on collinear manner. So, IA Fontan geometries have an increased chance of flow stagnation and a highly unsteady and dissipative interaction between the colliding flows, compared with that in EC geometries.

A quantitative comparison between two types of TCPC anatomies, EC and IA, was presented. Comparison between the TCPC geometries of these two models showed that it is area variation across the baffle length that is significantly different between the two surgical groups. Another major finding of this study was the narrowing of the LPA when compared with the RPA irrespective of the TCPC surgical technique in patients diagnosed with an HLHS. This suggests that the narrowing of the LPA may be attributed to the aortic reconstruction performed during the first stage of the Fontan surgery in HLHS patients. Clearly, HLHS patients are at a higher risk of exhibiting LPA stenosis, which calls for further investigation.

This study was funded by a BRP grant from National Heart, Lung, and Blood Institute (HL67622).

References

1. Fontan F, Baudet E. Surgical repair of tricuspid atresia. Thorax 1971;26:240–8.
2. Khairy P, Poirier N, Mercier LA. Univentricular heart. Circulation 2007;115:800–12.
3. de Zelicourt DA, Pekkan K, Wills L, et al. In vitro flow analysis of a patient-specific intraatrial total cavopulmonary connection. Ann Thorac Surg 2005;79:2094–102.
4. Deleval MR, Kilner P, Gewillig M, Bull C. Total cavopulmonary connection—a logical alternative to atriopulmonary connection for complex Fontan operations—experimental studies and early clinical-experience. J Thorac Cardiovasc Surg 1988;96:682–95.
5. Ensley AE, Lynch P, Chatzimavroudis GP, Lucas C, Sharma S, Yoganathan AP. Toward designing the optimal total cavopulmonary connection: an in vitro study. Ann Thorac Surg 1999;68:1384–90.
6. Pekkan K, Kitajima HD, de Zelicourt D, et al. Total cavopulmonary connection flow with functional left pulmonary artery stenosis: angioplasty and fenestration in vitro. Circulation 2005;112:3264–71.
7. Soerensen DD, Pekkan K, de Zelicourt D, et al. Introduction of a new optimized total cavopulmonary connection. Ann Thorac Surg 2007;83:2182–90.
8. Yang Y, Zhu L, Tannenbaum A, Giddens D. Harmonic skeleton guided evaluation of stenoses in human coronary arteries. Medical Image Computing and Computer Assisted Intervention 2005;8:490–7.
9. Zhu L, Haker S, Tannenbaum A. Flattening maps for the visualization of multibranched vessels. IEEE Trans Med Imag 2005;24:191–8.
10. Steele BN, Draney MT, Ku JP, Taylor CA. Internet-based system for simulation-based medical planning for cardiovascular disease. IEEE Trans Inform Technol Biomed 2003;7:123–9.
11. Paik DS, Beaulieu CF, Jeffrey RB, Rubin GD, Napel S. Automated flight path planning for virtual endoscopy. Med Phys 1998;25:629–37.
12. Wang KC, Dutton RW, Taylor CA. Improving geometric model construction for blood flow modeling. IEEE Eng Med Biol Mag 1999;18:33–9.
13. Antiga L, Steinman DA. Robust and objective decomposition and mapping of bifurcating vessels. IEEE Trans Med Imag 2004;23:704–13.
14. Kiesler K, Gugatschka M, Sorantin E, Friedrich G. Laryngotracheal profile: a new method for assessing laryngotracheal stenoses. Eur Arch Otorhinolaryngol 2007;264:251–6.
15. Rubin GD, Paik DS, Johnston PC, Napel S. Measurement of the aorta and its branches with helical CT. Radiology 1998;206:823–9.
16. Frakes DH, Conrad CP, Healy TM, et al. Application of an adaptive control grid interpolation technique to morphological vascular reconstruction. IEEE Trans Biomed Eng 2003;50:197–206.
17. Frakes DH, Smith MJ, Parks J, Sharma S, Fogel M, Yoganathan AP. New techniques for the reconstruction of complex vascular anatomies from MRI images. J Cardiovasc Magn Reson 2005;7:425–32.
18. Sanjeev S, Karpawich PP. Superior vena cava and innominate vein dimensions in growing children—an aid for interventional devices and transvenous leads. Pediatr Cardiol 2006;27:414–9.
19. Alexi-Meskishvili V, Ovroutski S, Ewert P, et al. Optimal conduit size for extracardiac Fontan operation. Eur J Cardiothorac Surg 2000;18:690–5.
20. Sluysmans T, Colan SD. Theoretical and empirical derivation of cardiovascular allometric relationships in children. J Appl Physiol 2005;99:445–57.